FINAL REPORT for GRANT NAG5–1558

TITLE: Global Electric Field Determination in the Earth's Outer Magnetosphere using Energetic Charged Particles

P.I. **Dr. Timothy E. Eastman**

Institution: University of Maryland

ph: 301–405–4829; email: eastman@glue.umd.edu

Co–I **Drs. R. Sheldon and D. Hamilton**
University of Maryland; Dr. C. McIlwain, UCSD

INDEX

INTRODUCTION

Although many properties of the Earth's magnetosphere have been measured and quantified in the past 30 years since it was discovered, one fundamental measurement (for zeroth order MHD equilibrium) has been made infrequently and with poor spatial coverage – the global electric field. This oversight is due in part to the neglect of theorists. However, there is renewed interest in the convection electric field because it is now realized to be central to many magnetospheric processes, including the global MHD equilibrium, reconnection rates, Region 2 Birkeland currents, magnetosphere-ionosphere coupling, ring current and radiation belt transport, substorm injections, and several acceleration mechanisms. Unfortunately the standard experimental methods have not been able to synthesize a global field (excepting the pioneering work of McIlwain's geostationary models) and we are left with an overly simplistic theoretical field, the Volland-Stern electric field model. Single point measurements of the plasmapause were used to infer the appropriate amplitudes of this model, parameterized by K_p (Maynard & Chen, 1975). Although this result was never intended to be the definitive electric field model, it has gone nearly unchanged for 20 years.

The analysis of current data sets requires a great deal more accuracy than can be provided by the Volland-Stern model. The variability of electric field shielding has not been properly addressed although effects of penetrating magnetospheric electric fields has been seen in mid-and low-latitude ionospheric data sets. The growing interest in substorm dynamics also requires a much better assessment of the electric fields responsible for particle injections. Thus we proposed and developed algorithms for extracting electric fields from particle data taken in the Earth's magnetosphere. As a test of the effectiveness of these new techniques, we analyzed data taken by the AMPTE/CCE spacecraft in equatorial orbit from 1984 to 1989.

Professor Carl McIlwain and colleagues of the University of California, San Diego participated in this work through a modest sub-contract. As described below, their research prepared key foundations upon which this research project is based and extensive discussions were held with Prof. McIlwain and colleagues to insure that our work built solidly on those foundations (see McIlwain, 1972; Whipple, 1978).

SPACECRAFT AND DATA SETS

The AMPTE/CCE spacecraft operated from launch on August 16, 1984 until early 1989. It was in a near equatorial orbit with an apogee of 8.8 R_E and a 15.6 h period. The spin axis of CCE points roughly sunward and its spin period is about 6 s.

A full complement of particle and fields instrumentation was flown as documented by Bryant et al. (1985). The primary instrument relevant to our study is the Charge-Energy-Mass Spectrometer (CHEM) which determines not only mass/charge but also the mass of ions from hydrogen to iron over an energy/charge range of ~1

to 310 keV/e in 32 equal logarithmic steps (see Gloeckler et al., 1985, for a full instrument description). CHEM uses a combination of electrostatic deflection and post acceleration of up to 30 kV followed by time-of-flight and energy measurements. Counts are accumulated and assigned onboard to a mass vs. mass per charge (M vs. M/Q) matrix that is then read out as matrix rates with specified ion species corresponding to particular sections of this matrix. More detailed information on composition, arrival direction, and ion energy is also made available through a direct pulse-height analysis system.

Additional instruments that provided data used in our study were the Medium-Energy Particle Analyzer (MEPA) (McEntire et al., 1985), the Magnetic Field Experiment (Potemra et al., 1985), and the Hot-Plasma Composition Experiment (HPCE) (Shelley et al., 1985). MEPA provided energetic ion measurements in several channels starting at 20 keV. HPCE provided two-dimensional measurements of electron velocity distributions from 50 eV to 25 keV and, for ion distributions, from near spacecraft potential to 17 keV/e . Simultaneous measurements of full magnetic field vectors are provided by the MAG instrument every 115 ms.

ANALYTIC TOOLS

To reconstruct the global electric field from single point measurements would require a large fleet of spacecraft which is currently not feasible. The CLUSTER spacecraft to be launched November, 1995 will address some of these issues but will not resolve the global character of the electric field from direct measurements. Thus we must rely on a secondary method, namely, using charged particles as tracers of the global fields with resolution time scales on the order of convection times, ~ hours. While this limits the method, it provides more than sufficient resolution for correlation with K_p, D_{st}, hourly AE, solar wind parameters and perhaps some substorm studies. This method has a long history and was used successfully by McIlwain (1972) to analyze geostationary satellite data . Thus we need a robust, efficient algorithm for extracting electric fields from particle data.

The usual approach is to integrate the guiding center equations with a sophisticated ordinary differential equation solver. This brute force method requires extensive CPU time (since the time steps have to be on the order of a gyroperiod) and traces one particle at a time. In order to describe the experimental data, many particles must be traced in order to build up a phase space density spectrum of the convecting particles. Because the final answer is nonanalytic, it is not extensible, parametric, or very predictive. Nor does it lend itself to an "invertible" algorithm for extracting the electric field. However there is an alternative method that makes use of the adiabatic invariants of the motion. In essence it is a Hamiltonian, energy-conserving approach to the problem in contrast to the usual Lagrangian integration-of-forces approach noted above.

Drift Motion in the Magnetosphere

The key to our adiabatic invariant approach is found in Whipple's seminal work on UB(K) coordinates (Whipple, 1978). For particles mirroring at the equator, and therefore lacking any parallel velocity, the total energy can be written as

Total Energy = Kinetic Energy + Potential Energy = μ B + qU

where μ is the first adiabatic invariant, B is the magnitude of the magnetic field, q is the particle charge state, and U is the electrostatic potential. Then tracing a particle's trajectory is merely finding the constant energy contours in the equatorial plane. The key insight from Dr. Whipple is that this same method works equally well for particles not mirroring at the equator as long as we replace B with B_m, the mirror point B magnitude. The second adiabatic invariant, J, and its relative K=J/SQRT(2 m μ) are conserved quantities of particle motion whereas B_m is not conserved. If dB/dt=0, our task is to find the dependence of B_m(K) and we can now trace the drift motion for any particle of given energy and pitch angle through the magnetosphere as shown in Figures 1 and 2.

A corollary to this approach arises from the invariance of three of the quantities in the above equation. Taking derivatives gives the relation dU/dB(K) = -μ/q. That is, if we transform our coordinates to U-B(K) space, the particle trajectories become straight lines whose slope depends only on their magnetic moment and charge. This coordinate space greatly simplifies our computer algorithm and furthers our intuitive understanding.

In implementing the B(K) mapping, we discovered that we had to define a more robust definition of K that would be defined on field lines with multiple minima. If we define a new K (and J) to be the sum over all trapped particle populations separated by possible intervening maxima on the field line, we recover a well behaved invariant for all field lines. This definition can be validated by testing for conservation of the total energy of the convecting particles which maintain this new invariant (see Figure 3).

A second corollary arises from the recognition that, although U-B(K) space is two-dimensional, the particles travel in essentially one dimension. The other dimension must then be identified with diffusion. (Since diffusion along the convection direction is essentially diffusion in drift phase, and because this information is lost in most steady state models, we retain only the perpendicular component.) Note that this diffusion entails no change in μ or K, maintaining the adiabatic invariants and thus the validity of the Hamiltonian approach. This provides a powerful way to disentangle the effects of convection from the effects of diffusion and thus resolve some of the inconsistencies in the standard diffusion model as found by Lyons and Schulz (1989). An illustration of these comparison is presented in Figure 5 which shows the deepest convection penetration for three species, H^+, He^+, and He^{++}, along with color-coded results using the ionospheric enhanced diffusion coefficient and the standard solar-wind driven diffusion coefficient.

Phase Space Density Evolution

The second key to our approach is quantifying the effect of convection on phase space density. This was first described by Wolf (1983) but only for equatorial mirroring particles. We generalize and rederive his result for all pitch angles. The reduced Vlasov equation integrated over gyrophase and bounce phase (an enhanced continuity equation) can be written as

$df(\mu, K)/dt + div(v\ f(\mu,K)) =$ charge exchange loss + diffusion + Coulomb drag

where f and v denote the distribution function and velocity, respectively. The second term becomes

$div(f(\mu,K)) = f(\mu,K)div(v) + v\ grad(f(\mu,K))$.

Using Whipple's derivation of the drift velocity on a constant K-surface, we obtain $div(v) = -v\ grad(B\ grad(K))/(B\ grad(K))$. Finally, combining this into the original equation and dividing by f gives

$$d(\ln f)/dt + v\ grad(\ln f\ /(B grad(K))) = \text{charge exchange rate} + \text{diffusion coefficient}/f + C\ d(\ln f)/d\mu$$

where C denotes the Coulomb drag coefficient. Space trajectory examples for different μ and K values are shown in Figure 4.

This master equation is very powerful. If we have a steady state solution so that the first term is zero, and if we neglect the right hand side, then the quantity f / (B grad(K)) remains constant along a drift trajectory. If the particles drift into a region of stronger B, they will also adiabatically have increased density as well. We now have the tools to describe the algorithm and data analysis below.

RESEARCH GOALS

Research goals for years 1 and 2 are listed below. We have met every one of the first year goals and substantially completed our second-year goals even though the research was descoped in funding by 15% for both years one and two and the proposed third year was not funded.

Our first year goals were to derive algorithms for extracting the electric field from an energetic particle data set. We have fulfilled every one of these goals. The first three (a-c) are semi-analytic algorithms unified in the C-language program CUB.C which will soon be available to all interested scientists through the National Space Science Data Center (NSSDC). Step d) involves data reduction which is unique to each data set though we outline the steps needed to extract the electric field from a time ordered, elliptical orbit data set. In step d' we anticipate the merged convection-diffusion model by producing a zeroth order fit to the entire data set incorporating both diffusion and convection electric fields.

Year 1 goals:

a) Given a model B -> extract K, $B_m(K)$

b) Given a model U -> find r,ϕ to U,B mapping

c) given a model U(K_p) -> plasmapause/Alfvén boundaries for each K_p

d) given a data set f(L) -> plasmapause/Alfvén boundary -> U

d') given a data set f(L) -> diffusion parameters

Limitations:

a) no losses in the convection (diffusion, coulomb drag)

b) superposition of two regimes, diffusion and convection

Our second year goals have been substantially completed. We completed analyzing nearly the entire four-year AMPTE/CCE/CHEM data set. This gives full radial and LT coverage of the trapping regions of the magnetosphere. It also extends the geomagnetic activity to incorporate the quietest periods of the last solar minimum as well as some of the major magnetic storms of the decade. We have not, however, compared our data with simultaneous measurements from other spacecraft although we were greatly encouraged to find similar analysis (and agreement) done with the CRRES data set. Although we have not done a systematic analysis using other ions species from the AMPTE/CCE/CHEM data set (count rates too low) or pitch angles (overly coarse in angular resolution), we have a case study involving pitch angle data from ISEE showing good agreement and consistency with the model (Sheldon, 1994).

Year 2 goals:

a) full radial/temporal coverage

b) self consistency checks with other E-field estimates

c) self consistency at boundaries

d) self consistency with other particle/pitch angles

e) extend the geomagnetic activity coverage

SCIENTIFIC ANALYSIS AND TESTS

Data Analysis and Testing

a) AMPTE/CCE/CHEM data analyzed for three satellite years

b) correlation of D_{st}, diffusion, K_p, convection E, LT, boundaries

c) time correlations of above

d) comparison with K_p and CRRES, DMSP satellites

The algorithms that we developed for scientific analysis are summarized in the "Software Tools" section below. Our work on these software tools has been important in several respects. Not only does it show the utility and generality of the subroutines,

but it is the first statistical study of diffusion in the ring current. This analysis enables new models to handle the full ring current thus going beyond the simple one-dimensional schematic ring current used by so many modelers (e.g., the Tsyganenko 89 magnetic field model). This can also be a building block for the NSSDC package of magnetospheric models, and perhaps can be profitably used in space weather, ionospheric modeling, and other applications in space environment studies.

The ring current is coupled quite effectively to the rest of the magnetosphere and can give us information about the previous history of the geomagnetic tail, reconnection rates, the occurrence frequency of substorms, and other key information on global magnetospheric response to changing solar wind or inner magnetospheric conditions. In a sense, the ring current is the prime "memory" of the magnetospheric system with each major storm or substorm leaving an imprint in the ring current.

Several global electric field models have been put forward which attempt to make the semi-empirical Volland-Stern model more self-consistent (Volland, 1978, del Pozo and Blanc, 1994). However, none of these models can be easily tested by conventional electric probe techniques. All direct measurement methods are single point determinations and they must somehow be averaged into a global picture without introducing a temporal bias. This is difficult enough without additional problems, introduced by the large gradients in plasma density and temperature seen in the magnetosphere, which introduce spurious spatial modulation of the signal. For example, the often cited Maynard-Chen correlation between K_p and electric field used the plasmapause crossings alone to determine the electric field, because at the plasmapause crossing the E-field probe went into saturation. This is essentially a particle measurement made with an E-field probe which was then used to infer the E-field! Thus particle measurements must be used to test these newer theoretical electric field models. This has not been done up to now primarily because these newer E-field models have been too complicated for the sort of analysis used by Maynard-Chen or CRRES. The advantage of the algorithms described in this report and generated through our Guest Investigator project is that they are easily implemented independent of the analytic complexity of the fields.

Inversion Algorithm for AMPTE/CCE/CHEM Data

The algorithm begins with a data set of measured phase space densities that can be binned in magnetospheric coordinates, preferably with measurements of the local magnetic field.

1) Phase space densities are normalized by dividing by (B grad(K)) where we have used an appropriate model for K. Since we are modelling lossless convection, and nearly lossless diffusion, we normalized the data again by dividing by the input spectrum at L=7.5 Re. Thus any changes to the input spectrum due to details of the plasmasheet acceleration would be removed from the fit.

2) Originally we were going to map the data from Energy-Time space into U-B space. But it turned out that it was much easier to manipulate the model than the data, which had data gaps and background contamination. Thus we chose a value for U and B, and calculated the Alfvén boundary, the boundary between convecting and diffusing ions. The use of different μ and K values enabled us to map this boundary at many different points in the magnetosphere. Large changes in the density are usually seen at this boundary, making it an important signal in the data. Then this boundary was calculated for several values of U, and mapped into E-T space. The best fit of the data with the model was calculated using a maximum likelihood indicator, chi-squared.

Figure 6 shows the automated fitting algorithm in action. The data are a single orbit with inbound and outbound passes illustrated. On the left are two panels, the first showing the location of the spacecraft vs. time, in L-shell and LT, and the second showing the upper boundary condition at L = 7.5 assumed for the fits. To the right are four energy-time panels showing, from top to bottom: raw data, log-smoothed data, diffusion fit, and diffusion fit with superposed convective signal. Note that the convective signal is much more intense than observed mainly because it assumes lossless convection from the plasmasheet. Note that the inbound convective signature extends down to L < 3, whereas the outbound convective signature extends only to L = 4. This is a result of two factors, LT dependence of convection boundaries and LT dependence of convection losses.

3) The "blur" at this boundary also tells us something about the diffusion rate, which in turn is related to the perturbation electric field. In this way, we get an estimate of power in the AC field in the appropriate frequency range in addition to a DC electric field. In practice, however, it was simpler to fit to the band of adiabatically energized protons which are diffusing in from the plasmasheet rather than the blurry boundary to find the appropriate diffusion coefficient which corresponds to the AC electric field.

The diffusion model over estimates the flux in some regions as shown in Figures 7. In particular, note that the data show a "meniscus" in the band of diffusing flux. This is not possible in steady state diffusion. Clearly a period of high diffusion has been followed by a period of low diffusion, and the 3 < L < 4 particles have longer persistence than 4 < L < 6 diffusing particles.

4) We have made a few iterations by hand, looking for the effects of a different U and B model. The B model dependence turned out to be small. The basic reason was that in the 3-5 R_E range of the Alfvén boundary, the magnetosphere is dominated by the dipole term, and the differences between Olson-Pfitzer or Mead-Fairfield are relatively minor. On the other hand, the electric field dependence was rather strong, and we generally found good convergence to a value for U.

Figure 8 shows some rather typical fits that we obtain with the present generation of the model and several problems remain with the fits. First, the real convective signal weakens with decreasing L-shell rather than increasing (due to adiabatic compression)

as in the model. This is a result of not having losses properly accounted for in the model. Second, the duskside orbits have a much cleaner Alfvén boundary signal than the dayside/dawn orbits, because the particles on the dayside have gone through perigee and are scattered or lost primarily by the hydrogen geocorona. Thus the signal is both weaker and more diffuse on the dayside. Clearly we must introduce losses into the model to correctly invert the dayside signals. Third, the time-dependence of the magnetosphere was never properly incorporated into the model leading to serious discrepancies in several regions, particularly in the diffusion regime.

The solution to the first problem is actually rather simple. If we consider Coulomb drag and charge exchange to be loss terms (rather than source terms) then we can associate a "decay time" with these loss terms. Then, in steady state, the observed density will just be the original value at the boundary (step 1) minus the particles lost on the way in from the boundary. In order to calculate the losses we need to know the convection time and the decay time. The convection time can be calculated from UB(K) coordinates using the Jacobian expression given in Whipple's 1978 paper. The decay time requires a loss cross section, a global neutral density model, and way to calculate the path-integrated losses. The cross section and density model have been incorporated into the program HEDIFF.FOR, whereas the path integration can be calculated as a byproduct of calculating $B_m(K)$ in the program CUB.C. However this calculation, although it now contains a time-dependent loss, remains a steady state solution.

The third problem is more complicated and will require the use of a time-dependent diffusion equation. Introducing time-dependence, however, destroys the invariance of the Alfvén boundaries. That is, particles that in a quiet magnetosphere were on closed orbits (diffusing) may suddenly find themselves on open orbits (convecting) or vice versa. This is the subject of Chen and Schulz's work at Aerospace (Chen et al., 1994). Chen's approach was to group all of these strange orbits into the class of "quasi-diffusing" ions, and to determine the phase space volume of this class of orbits through Monte-Carlo simulations of magnetic storms. The approach we favor is to combine both the convection and diffusion equations into a single master equation that has time dependence built in. The "quasi-diffusing" orbits can then be seen as a convection-cell assisted diffusion. It is expected that this equation will exhibit some of the characteristics of stochastic acceleration/chaos that are found in other non-linear dynamical systems. Perhaps this will then explain the acceleration of energetic ring current ions seen at Jupiter, for example. Clearly this last project is leading beyond the scope of the original grant.

Inversion Algorithm for ISEE 1 and 2 Data

The ISEE data used was collected from the two papers published by Dr. Donald Williams of JHU/APL using LEPEDEA and MEPI detectors (Williams and Frank,

1984; Williams et al., 1988). The data was presented in several formats, including Energy-Time spectrograms and line plots of pitch-angle distributions (see Figure 9).

1) From tabulations and plot axes, we determined the L-shell, radial distance, LT of the spacecraft where each spectrum was measured, as well as the prevailing values of K_p and D_{st}.

2) We examined the pitch angle plots to determine the magnetic moment μ of the observed peaks. Since Williams argues for a double peak in the data, we attempted to find a maximum and a minimum value of μ corresponding to these peaks.

3) We then constructed a UB(K) space transform, converting the location of the ISEE spacecraft into UB(K) coordinates using the information from step 1). We chose a value of the second invariant, K, to be consistent with the pitch angles observed. For each UB(K) map, we then found the intersection of the orbit associated with the most deeply penetrating plasmasheet ions with the actual spacecraft orbit, and tabulated the value of μ (or energy) at this point (see Figure 10).

4) There are essentially no free parameters in the model, yet we found remarkable agreement between the predicted values of μ and the observed values.

5) A second prediction made by our model is that the orbits of the most deeply penetrating plasmasheet ions depend on K or pitch angle. ISEE thus samples a succession of penetrating plasmasheet ion orbits of differing K values. This effect is manifest in the data as an evolution of the pitch-angle distribution from trapped "pancake" distributions to "dumbbell" pitch-angle distributions.

APPLICATIONS

Preliminary correlations from approximately one month of AMPTE/CCE/CHEM data (1985 days 130-160) show that the extracted electric field directly correlates with the extracted diffusion coefficient and that higher values of DC electric fields correspond to higher values of AC electric fields. Not surprisingly, the D_{st} index is positively correlated with the diffusion coefficient although it appears to be linearly correlated with the logarithm of the diffusion coefficient, an effect not previously observed. With the full data set analyzed through future work, it should be possible to extract a better formula for the D_{st} correlation (see Figure 11).

The extracted electric field did not agree very well with the K_p dependence of the Maynard-Chen model. At this point we are not sure whether our fits are in error or whether there is a large difference between global determination and single-point determination of the electric field. We note that Kerns et al. (1994) also found quite a bit of scatter in fits between a single point determination and a global determination. This may be the result of a bad model electric field (see del Pozo and Blanc, 1994).

Beyond the construction of the above algorithm, we envision applying this data set to the following problems:

1) A calculation of the divergence of current at the equator from the actual phase space densities and comparison with high-latitude parameters such as AE.

2) A calculation of the evolving phase space distribution with particular care in regions where the distribution is unstable leading to the growth of electromagnetic ion cyclotron or other plasma waves.

3) A correlation of electric fields with estimates of the reconnection rate from upstream monitors of the solar wind.

4) A correlation between electric field and substorm or storm progression, injection events, D_{st} and aurorae.

5) A correlation of electric field with ionospheric electric field measurements, penetrating electric fields, neutral winds, and f0f2. This pushes the maximum time resolution of the method which, in turn, depends on the orbit dynamics of the spacecraft used.

6) A correlation of electric fields measured with the 1-100 keV population with measurements of the cold plasmasphere distribution, location of the plasmapause, and whistler observations.

BIBLIOGRAPHY

Bryant, D. A., S. M. Krimigis, and G. Haerendel, Outline of the active magnetospheric particle tracer explorers (AMPTE) mission, IEEE Trans. on Geosci. and Remote Sensing **GE-23**, 177, 1985.

Chen, M. W., L. R. Lyons, and M. Schulz, Simulations of phase space distributions of storm time proton ring current, *J. Geophys. Res.* **99**, 5745, 1994.

del Pozo, C. F., and M. Blanc, Analytic self-consistent model of the large-scale convection electric field, *J. Geophys. Res..*, **99**, 4053, 1994.

[M.-C. Fok, et. al, "Decay of Equatorial Ring Current Ions and Associated Aeronomical Consequences", JGR , 98, 19,381, 1993]

Gloeckler, G., F. M. Ipavich, W. Studemann, B. Wilken, D. C. Hamilton, G. Kremser, D. Hovestadt, F. Gliem, R. A. Lundgren, W. Rieck, E. O. Tums, J. C. Cain, L. S. Masung, W. Weiss, and P. Winterhof, The charge-energy-mass spectrometer for 0.3–300 keV/e ions on the AMPTE CCE, IEEE Trans. on Geosci. and Remote Sensing **GE-23**, 234, 1985.

Kerns, K. J., D. A. Hardy, and M. S. Gussenhoven, Modeling of convection boundaries seen by CRRES in 120–eV to 28–keV particles, *J. Geophys. Res.* **99**, 2403, 1994.

Lyons, L. R., and M. Schulz, Access of energetic particles to storm time ring current through enhanced radial "diffusion", *J. Geophys. Res..*, **94**, 5491, 1989.

Maynard, N. C., and A. J. Chen, Isolated cold plasma regions: Observations and their relation to possible production mechanisms, *J. Geophys. Res.* **80**, 1009, 1975.

McEntire, R. W., E. P. Keath, D. E. Fort, A. T. Y. Lui, and S. M. Krimigis, The medium-energy particle analyzer (MEPA) on the AMPTE CCE spacecraft, IEEE Trans. on Geosci. and Remote Sensing **GE-23**, 230, 1985.

McIlwain, C. E., Plasma convection in the vicinity of the geosynchronous orbit, in *Earth's Magnetospheric Processes,* B. M. McCormac, ed., D. Reidel Publ. Co., pp. 268–279, 1972.

Olson, W. P., K. A. Pfitzer, and G. J. Mroz, Modeling the magnetospheric magnetic field, in *Quantitative Modeling of Magnetospheric Processes,*, Geophys. Monogr. Ser. Vol. 21, edited by W. P. Olson, pp. 77–85, American Geophysical Union, Washington, D.C., 1979.

Potemra, T. A., L. J. Zanetti, and M. H. Acuna, The AMPTE CCE magnetic field experiment, IEEE Trans. on Geosci. and Remote Sensing **GE-23**, 246, 1985.

Richmond, A. D., M. Blanc, B. A. Emery, R. H. Wand, B. G. Fejer, R. F. Woodman, S. Ganguly, P. Amayenc, R. A. Behnke, C. Calderon, and J. V. Evans, An empirical model of quiet-day ionospheric electric fields at middle and low latitudes, *J. Geophys. Res..*, **85**, 4658, 1980.

Sheldon, R. B., Plasmasheet convection into the inner magnetosphere during quiet conditions, in *Initial Results from STEP Facilities and Theory Campaigns,* Proceedings of the 1992 COSPAR Colloquium, D. N. Baker ed., Pergamon Press, N.Y., pp. 313–317, 1994.

Shelley, E. G., A. Ghielmettic, E. Hertzberg, S. J. Battel, K. Altwegg von Burg, and H. Balsiger, The AMPTE/CCE hot-plasma composition experiment (HPCE), IEEE Trans. on Geosci. and Remote Sensing **GE-23**, 241, 1985

Stern, D. P., A study of the electric field in an open magnetospheric model, *J. Geophys. Res..*, **78**, 7292, 1973.

Volland, H. A., A semiempirical model of large-scale magnetospheric electric fields, *J. Geophys. Res..*, **78**, 171, 1973.

Volland, H. A., A model of the magnetospheric-ionospheric electric field, *J. Geophys. Res..*, **83**, 2695, 1978.

Whipple, E. C., (U,B,K) coordinates: A natural system for studying magnetospheric convection, *J. Geophys. Res..*, **83**, 4318, 1978.

Williams, D. J., and L. A. Frank, Intense low-energy ion populations at low equatorial altitudes *J. Geophys. Res..*, **89**, 3903, 1984.

Williams, D. J., W. Lennartson, and L. A. Frank, Low-energy ions at low equatorial altitudes, *Planetary and Sp. Sci..*, **36**, 703, 1988.

Wolf, R. A., The quasi-static (slow-flow) region of the magnetosphere, in *Solar Terrestrial Physics: Principles and Theoretical Foundations*, ed. by R. L. Carovillano and J. M. Forbes, D. Reidel Publ. Co., pp. 303–368, 1983.

GRANT PUBLICATIONS

We have published four publications under this grant. In addition, there are many related publications by the investigators and works directly motivated by this grant activity as documented below.

1. Sheldon, R.B. and J.D. Gaffey Jr., Particle Tracing in the Magnetosphere: New Algorithms and Results, *Geophys. Res. Lett.*, **20**, 767–770, May, 1993.

This paper outlines the algorithmic technique that enables us to find convection paths of ions through the magnetosphere with an order of magnitude more accuracy and an order of magnitude greater speed. It also predicts additional trapping regions for low energy ions, and makes the first-ever prediction of deeply penetrating warm plasmasheet ions.

2. Sheldon, R. B., Plasmasheet convection into the inner magnetosphere during quiet conditions, in *Initial Results from STEP Facilities and Theory Campaigns*, Proceedings of the 1992 COSPAR Colloquium, D. N. Baker ed., Pergamon Press, N.Y., pp. 313–317, 1994.

This paper applies the algorithms of the first paper to unexplained observations made by the ISEE instrument (Williams and Frank, 1984) showing that our predicted signature of deeply penetrating plasmasheet ions is precisely what was observed. These results demonstrate not only the convenience and power of the new method but also the necessity of using a Hamiltonian approach.

3. Sheldon, R. B., and D. C. Hamilton, Ion Transport and Loss in the Earth's Quiet Ring Current 2. Diffusion and Magnetosphere-Ionosphere Coupling, *J. Geophys. Res..*, **99**, 5705–5720, 1994.

This continues previous work on ring current diffusion using the new algorithm to separate the data into well-behaved diffusive or convective regimes. The primary result of the paper concerns the AC modulation of electric fields rather than the DC component but the results were made possible by increased understanding of the convective contribution to diffusion (see Figure 11).

4. Sheldon, R. B., and T. E. Eastman, Ion transport and loss in the Earth's quiet ring current 3. Convection and diffusion, submitted to *J. Geophys. Res..*, Feb. 1995.

This work brings together two separate descriptions of the magnetospheric trapped particles by considering both the diffusion and convection contributions of the ring current. With greater insight into the mechanisms that produce the ring current, it is hoped that some of the outstanding questions concerning ring current formation and decay can finally be answered.

During the 3–1/2 year period that this Guest Investigator project was in effect, a significant part of the data analysis and modeling was carried out by co-investigator, Dr. Robert Sheldon, now with the University of Bern, Switzerland. From August, 1991 through January, 1994, the Principal Investigator, Dr. Eastman, was on leave-of-

absence to the National Science Foundation as Program Director for Magnetospheric Physics [2–1/2 years at NSF and just over one year full-time at the University of Maryland during the active grant period]. During the active period of this grant, the P.I. presented a total of 20 invited lectures and published 10 papers, including six as first author (some are listed below under related publications and invited lectures). While at NSF, Dr. Eastman played the lead role in conceiving and initial forwarding of the important Space Weather Initiative (building on the NSF-STEP initiative that he formulated), managed and expanded the Geospace Environment Modeling (GEM) program, and provided coordination at NSF for all aspects of plasma science and technology.

Works Directly Motivated by this Study:

The influence of this work has to be inferred from the literature partly because electric fields and ring current have not been in the limelight in recent years.

The work of Chen and Schulz (Chen et. al., 1994) in which they simulated the electric fields seen during a magnetic storm and then analyzed the effects on a model ring current originally used a Lagrangian approach and lots of computer time. After their first papers, they have switched to a Hamiltonian approach although they use a completely different analytic (and simplified) description of the magnetic fields.

The work of Bob Langel on magnetic field anomalies uses the methods of geophysics (spherical harmonic decomposition of Earth's main field) to analyze magnetometer data on near earth satellites. This is very similar to the work of Nicolai Tsyganenko who has concentrated more on the geotail and satellites in high-altitude orbits. Langel rediscovered that the ring current had an asymmetric B-field signature, which is sometimes confused with the asymmetric ring current seen during storms. However this asymmetric B-field signature existed for quiet magnetospheric conditions as well. This asymmetry has been published before though the literature does not contain any explanation. Using the invariance of f/[B grad(K)], we were able to show that a convection electric field adiabatically compresses the ring current on one side of the magnetosphere creating higher currents and an asymmetric B-field. In this situation, the concepts are not new but the simplicity of this UB(K) approach greatly facilitated the explanation. We note that Sugiura works very hard to remove any asymmetric component to the D_{st} index which, in this case, is unfortunate since this component contains information about the convection electric field (see Figure 12).

The work of Fok et al. (1993) on the decay of the ring current due to Coulomb drag and charge exchange continues to use a Lagrangian approach, primarily because an integration-of-forces technique depends explicitly on time so that loss processes can be easily included. This "failure" of the Hamiltonian approach to include time-dependence points out the need for a time-dependent Hamiltonian description of both

convection and diffusion which will be general enough to include losses. This is a key element of our fourth paper (see Grant Publications above).

The work of Kerns et al. (1994) is fascinating because they had very similar goals to ours: analyzing the entire CRRES data set for electric fields. The method they used is nearly identical to that of McIlwain's pioneering ATS6 analysis and very similar to Maynard and Chen (1975). Namely, they identify the Alfvén boundaries using both electrons and low energy (< 10 keV) protons. From this boundary they then infer the appropriate Volland-Stern electric field. One innovation was to use both a dipole magnetic field and an Olson-Pfitzer magnetic field in their fits showing that a more "modern" magnetic field model produced a better fit in most cases. However, it was not clear whether their analytic method of inverting the Alfvén boundaries was generally enough because only two fits were shown. This is unfortunate because this data set could have been used to greatly improve the empirical determination of electric and magnetic fields.

Other Related Publications by the P.I.:

Eastman, T. E., Transition regions in solar system and astrophysical plasmas, *IEEE Trans. Plasma Science,* **18**, No. 1, 18–25, 1990.

Eastman, T. E., E. A. Greene, S. Christon, G. Gloeckler, D. C. Hamilton, F. M. Ipavich. G. Kremser, and B. Wilken, Ion composition in and near the frontside boundary layer, *Geophys. Res. Lett.,* **17**, 2031–2034, 1990.

Eastman, T. E., Recent ion composition results in the magnetopause region, in *Physics of Space Plasmas (1991),* SPI Conference Proceedings and Reprint Series, Number 10, T. Chang, G. B. Crew, and J. R. Jasperse, eds., Scientific Publishers, Cambridge, MA, pp. 209–218, 1991.

Eastman, T., Micro- to macroscale perspectives on space plasmas, *Physics of Fluids B* (Plasma Physics), **5**, 2671, 1993.

Eastman, T., Magnetosphere, submitted with invitation to *The Encyclopedia of Climate and Weather,* Oxford University Press, 1994.

Eastman, T. and S. P. Christon, Ion composition and transport near the Earth's magnetopause, in *The Physics of the Magnetopause,* P. Song, B. Sonnerup, and M. Thomsen, eds., AGU, Washington, D.C., in press, 1995.

Eastman, T. E., D. C. Hamilton, S. A. Fuselier, and J. T. Gosling, Magnetopause crossings without a boundary layer, submitted to *J. Geophys. Res.*, Feb., 1995.

Invited Lectures by the P.I. Related to this Study:

Emerging perspectives on the magnetopause and frontside boundary layer, MIT, July, 1990.

Reviews of magnetospheric boundary layers and new results from AMPTE/CCE, SwRI, Dec., 1990.

Ion composition near the dayside magnetospheric boundary, Dartmouth, May, 1991.

Geospace: our laboratory for space plasma kinetics, MIT, Aug., 1992.

Micro- to macroscale processes in Geospace, APS meeting, Seattle, Nov., 1992.

Global coherence and cross-scale coupling in the Earth's magnetosphere, Fall AGU, Dec., 1993.

Composition and microstructure in the magnetopause region, Chapman Conf., San Diego, Mar., 1994.

SOFTWARE TOOLS DEVELOPED THROUGH GRANT SUPPORT

The three software tools we have developed are general enough to use for other data sets and ISTP analysis. We give a more detailed description of each program below.

a) UBK calculation program CUB.C

b) Fitting program ET.PRO

b') MaxMin.PRO

c) Diffusion Modelling program HEDIFF.FOR

CUB.C is a C-language program that calculates all trajectories of a specified 2nd invariant in the equatorial plane. That is, for a given configuration of magnetic and electric field, all possible trajectories of particles for arbitrary energy, charge state, and/or starting position can be calculated globally in seconds. Naturally, the initialization of the polynomials representing the magnetic field of the mirror point as a function of pitch angle requires several hours of SUN Sparc1 CPU time, however, this need only be done once for a given magnetic field configuration. The Hamiltonian approach is not only faster but also more accurate than a traditional Lagrangian integration approach.

The program incorporates 7 parametrically-adjustable magnetic field models (Tsyganenko 87, Tsyganenko 89, Olson-Pfitzer 88, Mead-Fairfield, McIlwain M2, IGRF85 and Dipole) and 3 electric field models (Volland-Stern, McIlwain E5, Richmond 80), so that cross comparisons and "best-fit" models can be found. It demonstrates the true universality of the Hamiltonian method which does not require analytic approximations to a dipole field or any simplifications to the models. This is in complete contrast to the literature where simplified approximations to a dipole-like field are a necessary first step toward making the Lagrangian approach tractable (Kerns et al., 1994, Chen et al.,1994). Note however that the results of Paper 2 depend critically on realistic field models that can explain the features seen in the data.

ET.PRO is a series of IDL [Interactive Data Language, Research Systems, Inc., Boulder, CO] routines that read in energy-time ordered data, normalize it, and compare it with standard diffusion and convection "fits" using a maximum-likelihood technique. There are several advantages to this approach. First, it is able to rapidly process a large data set consisting of several hundred orbits and is easily generalized to any spacecraft data set. Second, it is capable of (nearly infinite) refinement by increasing the number of "example fits" for comparison. Third, the method is deterministic and does not require convergence to a minimum of a complicated function. Fourth, the method is less subject to bias because an objective "goodness-of-fit" criterion is used to select the appropriate fit rather than a more arbitrary "chi-by-eye" subjective criterion. The limitations of the method are those pitfalls common to any modelling, that an appropriate model fit must be used or else the "best-fit" model will not resemble reality.

MAXMIN.PRO is a subroutine of ET.PRO that models the motion of the spacecraft in transformed UB(K) coordinates, calculating precisely the intersection of the spacecraft with Alfvén boundaries at each time step. This is important because it is these boundaries that produce "features" in the data, and a zeroth-order fit must match the model spectra with these data "features". The method is essentially geometrical and is a great simplification both conceptually and algebraically compared to the usual method of finding these boundaries in a data set as exemplified in a very similar analysis done with CRRES data by Kerns et al. (1994).

HEDIFF.FOR is a FORTRAN program that solves the diffusion partial differential equations for hydrogen and helium, incorporating both Coulomb and charge-exchange losses. The diffusion equation solves only the steady state situation, and thus is limited to periods when the magnetosphere changes little on the timescale of a half-orbit (8 hours). Although this would seem to restrict the applicability of the model, in practice it picks out the maximum diffusion seen during a given orbit which is still a useful description of the magnetosphere.

This last program was developed primarily under a separate NASA grant but we include it here because it was essential in producing the fits used in ET.PRO and because important modifications were made for this grant project.

Report on the University of Maryland contract to UCSD under NASA Grant NAG5-1558, T. E. Eastman Principal Investigator

History

The data from the UCSD instrument on the ATS-5 spacecraft in geosynchronous orbit revealed the dispersion patterns of the particles injected each magnetospheric substorm. The paths followed by the injected particles not only depend upon the particle's location, energy/charge, and pitch angle, but also the magnetospheric magnetic and electric fields. The difficult task of using the dispersion patterns to deduce the magnetospheric electric field was found to be greatly aided by using adiabatic constants of motion (McIlwain, 1972, 1974) in a way in which trajectories were transformed into straight lines. E. Whipple of UCSD formalized and generalized this technique with the introduction of the U-B-K coordinate system (Whipple (1978).

Application to non-Geosynchronous Spacecraft

The analysis of data from spacecraft in non-circular inclined orbits is considerably more complex than the analysis of data from geosynchronous spacecraft. The U-B-K coordinate system, however, is again a powerful tool when solving the inverse problem of deducing the electric field patterns from dispersion patterns observed along such orbits.

The role of UCSD in this grant has been to study this more generalized use of the U-B-K coordinate system in order to assist and advise the Principal Investigator in the analysis of data from spacecraft such as the AMPTE/CCE. This assistance has been provided during informal discussions during various AGU meetings, and the 1992 GEM meeting in Snowmass Colorado. An informal meeting with R. Sheldon was held at the Goddard Spaceflight Center in October 1991 with E. Whipple and T. Northrup also in attendance. Extensive discussions were held during a visit to the University of Maryland in January 1993. The topics of these discussions included various aspects of building upon techniques previously developed at UCSD for taking advantage of the U-B-K coordinate system in light of the specific characteristics of the data from the AMPTE/CCE CHEM instrument. Also discussed at length were various possible ways to extend adiabatic theory to include the effects of radial diffusion.

Dr. Yuri Galperin from the Space Research Institute in Moscow (IKI) received partial support from the UCSD subcontract during a two month visit to UCSD in the summer of 1992. Dr. Galperin had independently developed techniques for using adiabatic theory in the interpretation of experimental data. He was thus able to bring fresh insights into the discussions held at UCSD and at the 1992 GEM meeting.

C. E. McIlwain

C. E. McIlwain
Research Professor
University of California, San Diego

CAMPUS: UMCP

UNIVERSITY OF MARYLAND
CONTRACTS AND GRANTS SYSTEM
ATS/INPUT FORM

12/09/92

NOTATION: ADD TIME

FAS-NUMBER: 01-5-26045

SPONSOR: 10 NASA

SUB-DIVISION: GODDSPAFLICE

AGR/PRP-NUMBER (AGENCY): NAG 5-1558

DIRECTOR: EASTMAN, DR. T.

DIV: 1L COMPUTER, MATH & PHYSICAL SCI

DEPART: 11L080 INST PHY SCI TH

AMOUNT: 0000000000 TITLE: GLOBAL ELECTRIC FIELD DETERMINATION IN THE...

START-DATE: 05-15-91 EXPIRE-DATE: 05-14-94 COMP NUMBER ASSIGNED: 1037174A

PREVIOUS ID NUMBER, IF APPLICABLE: _____

S.A.I. NUMBER: MD ____-____-360201

RELATED ACCT #: _____ FUNDS:

PREVIOUS ACCT #: _____ THIS ACTION * : 0

INDIRECT COST RATE : 46% MTDC PREVIOUS ACTION(S) : 123,000.00

RENEWAL/CONTINUATION: to be submitted: 01-14-94 TOTAL : 123,000.00

* DIRECT COST THIS ACTION : 0

PROJECT REPORTS: SEMI-ANNUAL PROGRESS REPORTS, FINAL TECHNICAL AND PATENT REPORTS.
(Financial reports will be prepared by Office of Contract and Grant Acctng.)

P.D. EFFORT- This agreement reflects: DR. T. EASTMAN 1.0 MONTHS.

COST SHARING: NONE.

REMARKS: A COPY OF AWARD ATTACHED FOR MS. E. GALIFARO.

REPORTS: PLEASE SEND A COPY OF TRANSMITTAL OF ALL REPORTS.
TO THE OFFICE OF RESEARCH ADMINISTRATION & ADVANCEMENT.

ASSISTANCE: Administration BOOKER. T. MCMANUS Extension 5-6269
Accounting DENNIS TRIMBLE Extension 5-2607

FIGURES

1. An equatorial cut in the X-Y plane to UB(K) mapping for a dipole magnetic field plus Volland-Stern (Volland, 1973; Stern, 1973) shielded electric field appropriate for K_p=0 (Maynard and Chen, 1975). Lines of tangency between contours of constant B and U are shown dotted. Dash-dotted line converts B_m to radial distance with the right-hand scale. The plasmapause, the last closed 0.0 eV/nT trajectory, is bracketed by solid lines. The open drift trajectory that penetrates most deeply into the magnetosphere is bracketed by dashed lines. With a slope of 19.2 eV/nT, it follows a banana orbit but only crosses a tangency line once, at dusk close to the earth (from Sheldon and Gaffey, 1993).

2. Equatorial X-Y to UB(K) mapping for realistic Olson-Pfitzer (Olson et al. 1979) magnetic field and Volland-Stern (K_p) plus ionospheric dynamo (Richmond et al. 1980) electric fields. Top panels calculated for 90° pitch angles, K=0; bottom panels for K=100. The extra loop in X-Y tangency curves generated by a quadrupolar ionospheric field becomes a topological pleat in UB(K) space. Trajectories labeled similarly as in previous figure. Dashed "most deeply penetrating" trajectory has a slope of 10.2 eV/nT in top panels, 20.2 eV/nT in bottom panels (from Sheldon and Gaffey, 1993).

3. a) Field lines traced from the equatorial plane at 10 R_E with longitude varying from midnight to noon in 20° increments; b) K(s) for field lines at 10 R_E; c) B_m(K), which is well defined for all field lines; and d) B(s) for field lines at 10 R_E with an off-equatorial minimum in the noon field line (from Sheldon and Gaffey, 1993).

4. a) X-Y space trajectories for μ=10 eV/nT, K=0; b) X-Y space trajectories for μ=10 eV/nT, K=100; c) K=100 equatorial pitch angles α, contours every 2°; d) Relative phase space density proportional to $B_m(K)/\mathrm{sqrt}[\mu\ (B_m(K) - B_{eq})]$ for μ=10 eV/nT, K=100 (from Sheldon and Gaffey, 1993).

5. The deepest convection penetration is displayed along with model results for the ionospheric enhanced diffusion coefficient and the standard solar-wind driven diffusion coefficient for three magnetospheric species in 3 rows; protons, He^+ and He^{++}. The first column color codes particles that begin at L > 7 (red) or L < 3 (blue). Thus the red region contains the deeply-penetrating plasmasheet ions and thus delimits the region for which the standard diffusion model does not strictly apply. The boundary between these convecting orbits and the stably trapped orbits is the Alfvén boundary which, for zero energy, would be the plasmapause. Note that this boundary is somewhat fuzzy for L >3 producing a region of enhanced diffusive transport (from Sheldon and Hamilton, 1994).

6. This figure illustrates the automated fitting algorithm in action. The data are a single orbit, with inbound and outbound passes plotted. On the left are two panels, the first showing the location of the spacecraft vs. time, in L-shell and LT, and the second showing the upper boundary condition at L=7.5 assumed for the fits. To the right are 4 energy-time panels showing from top to bottom: the logarithms of the raw data, the log-smoothed data, the diffusion fit, and the diffusion fit with superposed convective signal. Note that the convective signal is much more intense than observed mainly because it assumes lossless convection from the plasmasheet. Note that the inbound convective signature extends down to L < 3, whereas the outbound convective signature extends only to L=4. This is a result of two factors – LT dependence of convection boundaries and LT dependence of convection losses.

7. Energy-time proton spectrograms for outbound pass 1985 day 217 with log scaling of intensities. Top panel is raw data; note that steps 0-4 were measured in a different mode than channels 6-31 and the counting efficiency as well as calibration changes dramatically at step 5. Since steps 0-4 are generally contaminated with background, we include them only cautiously and smooth the boundary between the two modes. The second panel shows the effect of a 3–point average of the logarithms of the flux. This smoothing also produces a much better fit to the diffusion model in panel 3. We superpose a lossless convection profile using the boundary condition at L=7.5 to produce panel 4. Comparing with panel 1, we see that intense fluxes are observable in the convection band but with low probability of detection. This is partly due to the narrowness (energy and time) of the convecting flux and the lengthy duty cycle of the instrument.

8. Energy-time proton spectrogram for outbound pass 1986 day 324 with log scaling of intensities as above. Note that the diffusion band (green diagonal band from upper left to lower right) exhibits a thinning or meniscus around L=6. This cannot be reproduced from any steady-state diffusion model but is characteristic of time-dependent diffusion. Note also that the convection signature extends down below L=3, at LT=1500. This is the best local time for detecting the convection particles and produces the best fits. Again, we model convection without losses which account for the large difference in intensity of the measured vs. predicted convection band.

9. Combined MEPI and LEPEDEA spectra are presented here (from Williams and Frank, 1984). LEPEDEA data points assume q=1 and MEPI data points assume protons. Several energy peaks can be seen. Note the disagreement between the lowest MEPI energy channel (24.0–34.2 keV) and the higher LEPEDEA channels. Because of the MEPI finite proton detection efficiency for energies < 24 keV and the presence of a steep spectral gradient at ~20 keV, the 24.0–34.2 keV MEPI data

point should be plotted at a lower energy and within the spectral gradient region.

10. Deepest penetration is illustrated here for three energies. A moderately quiet magnetosphere mapped into U,B coordinates with three energy-dependent trajectories (at 90° pitch angle, K=0) demonstrating the ease with which the most deeply penetrating trajectory can be found using only geometrical constraints.

11. We have processed approximately 40 days of AMPTE/CCE/CHEM orbits and plot their statistics in four panels vs. fitted diffusion coefficient displayed in a logarithmic format. The top panel displays the number of cases in each bin showing that the ring current has an exponential distribution of diffusion strengths much like the distribution of K_p. The second panel shows that enhanced diffusion (AC) is correlated with enhanced convection (DC). The third panel shows that there appears to be linear correlation between K_p and the log of the diffusion coefficient strength which is not surprising because K_p is a logarithmic index as well. The fourth panel shows the there is linear trend with D_{st} as well which is more surprising because D_{st} is a linear indicator, not a logarithmic indicator.

12. Local time effects on energy density and number density: An average quiet time ring current profile is shown in four local-time quadrants using the energy channels 1-310 keV/q from the AMPTE/CCE/CHEM quiet-day data set. The energy-density profile contains > 90% of the total energy in the ring current for L-shells > 3. The number density is dominated by the lowest energy particles and therefore may greatly underestimate the total number density. Note that the midnight quadrant dominates the energy and number density for L-shells > 6 in keeping with the plasmasheet origin, whereas the dusk quadrant dominates the energy and number density for L-shells $3 < L < 5.5$ due to convection electric field compression of the ring current. This effect produces an asymmetry in the B-field magnitude as measured at equatorial latitudes even for quiet ring current.

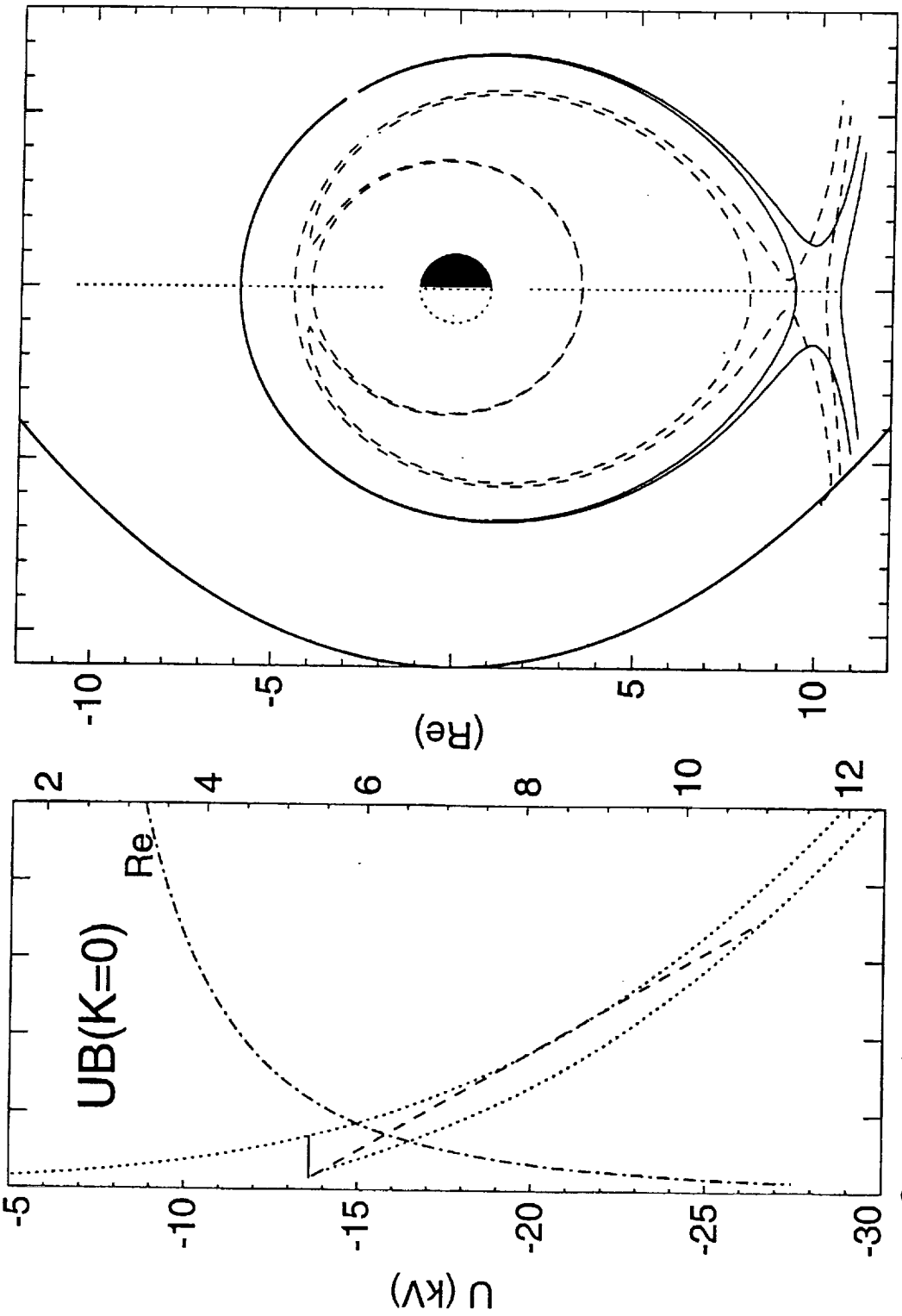

FIGURE 1.

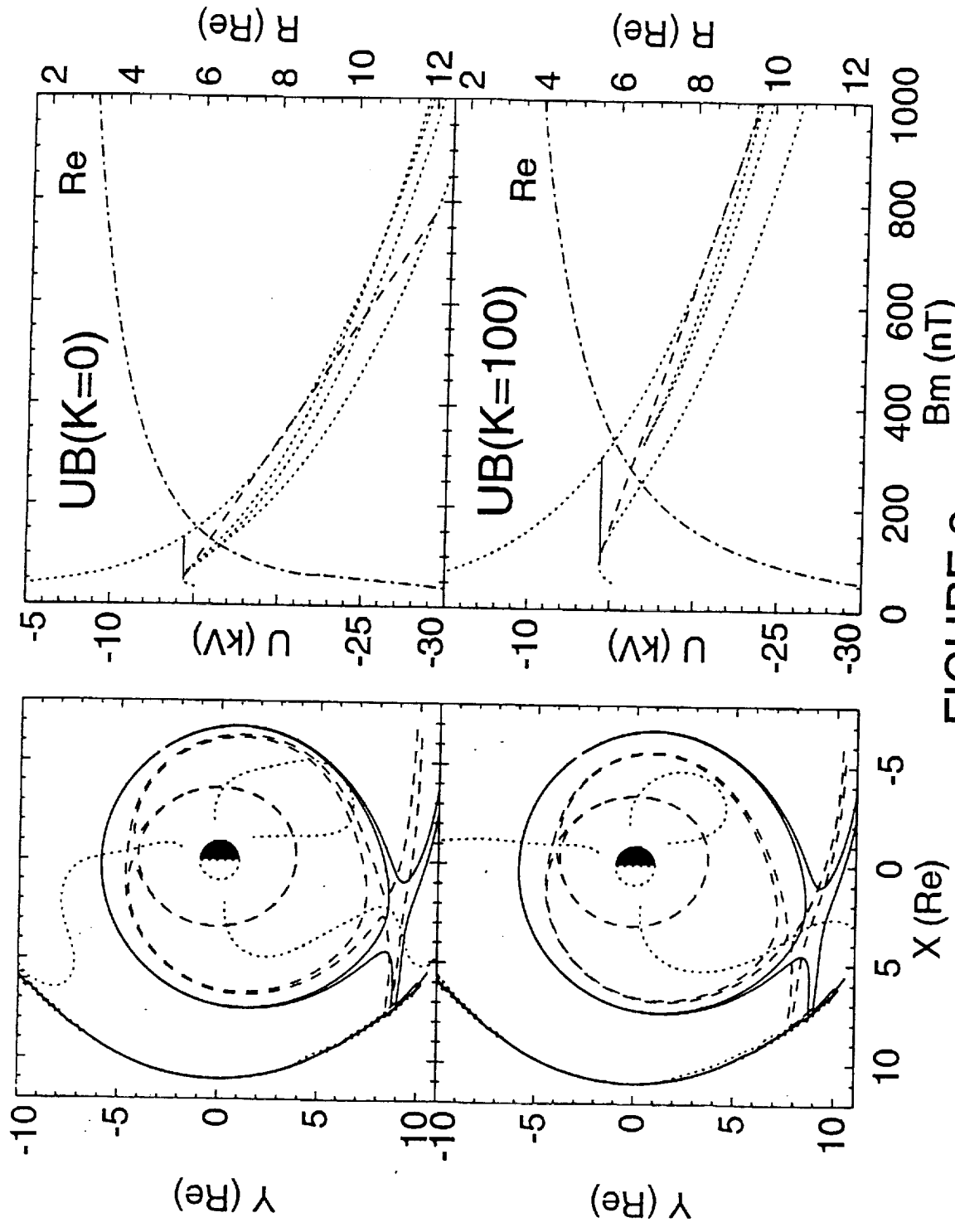

FIGURE 2.

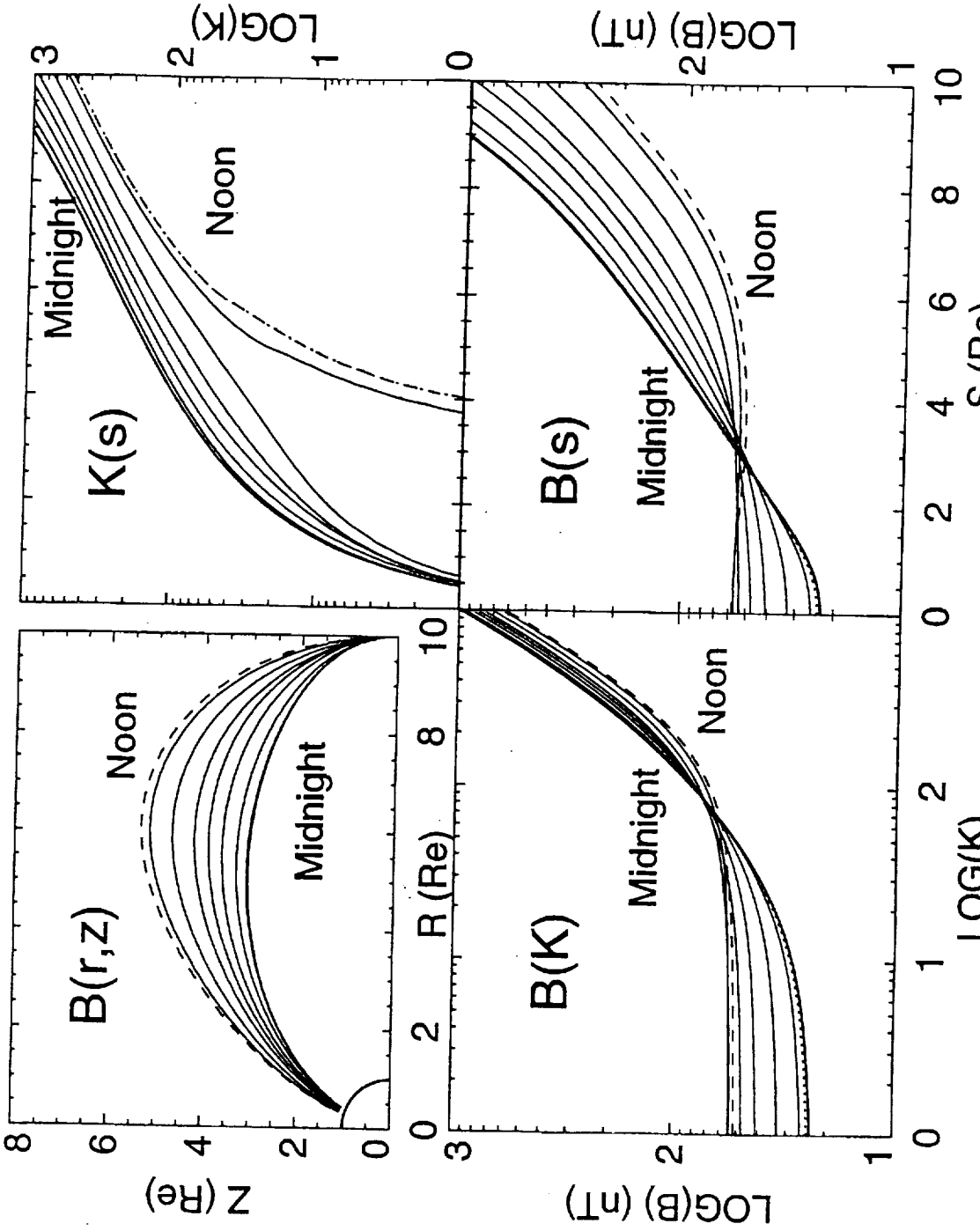

FIGURE 3.

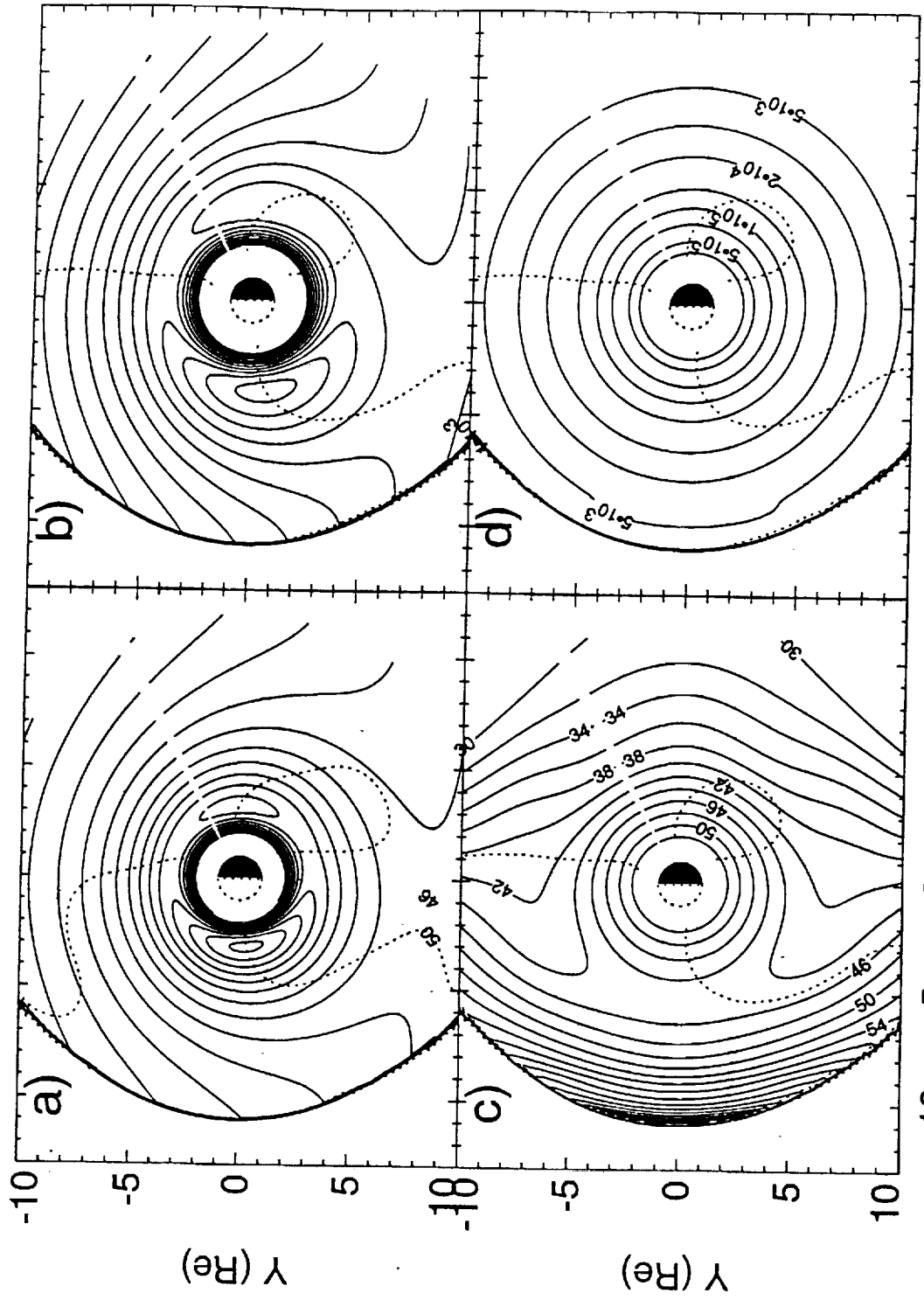

FIGURE 4.

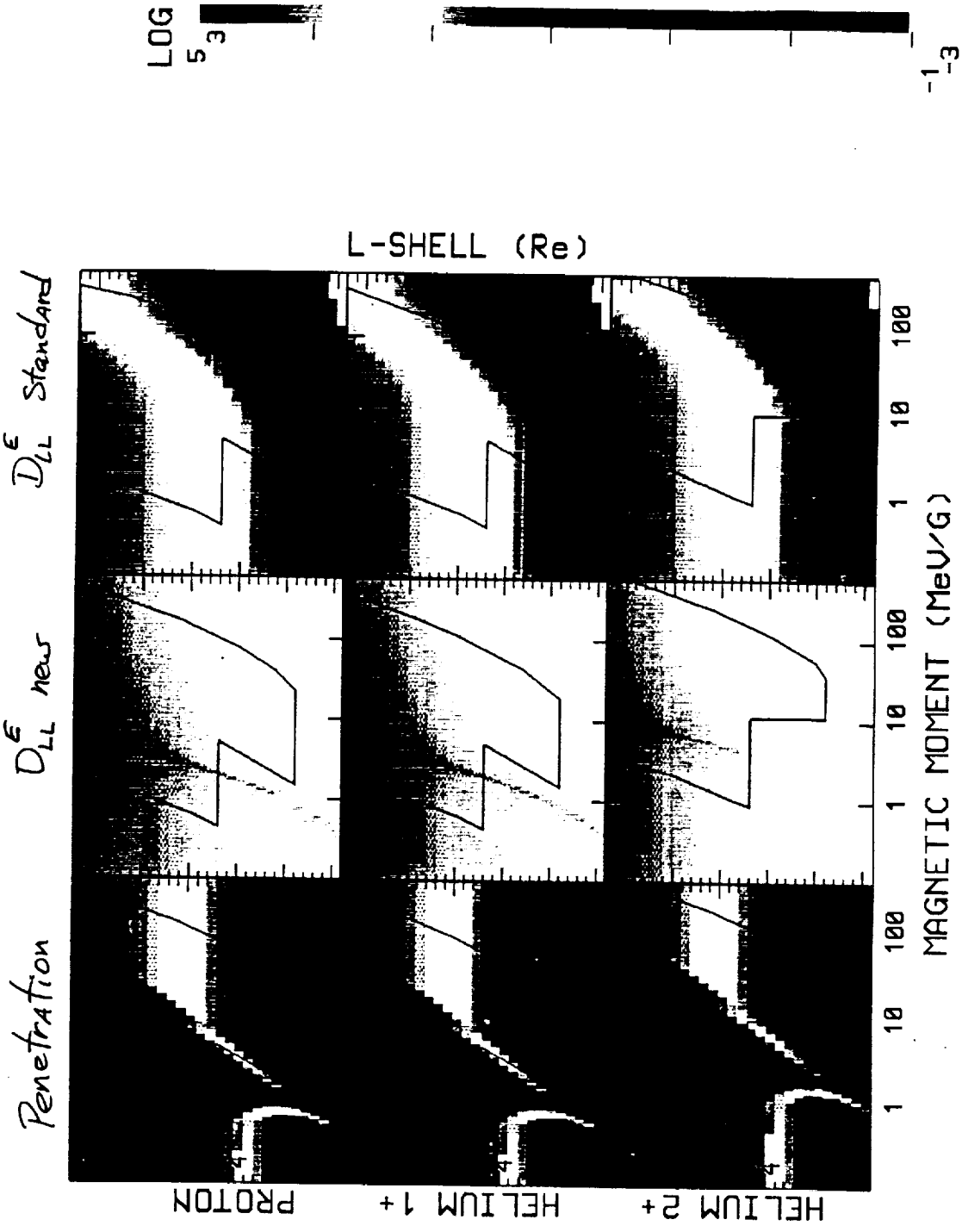

FIGURE 5 (original in color)

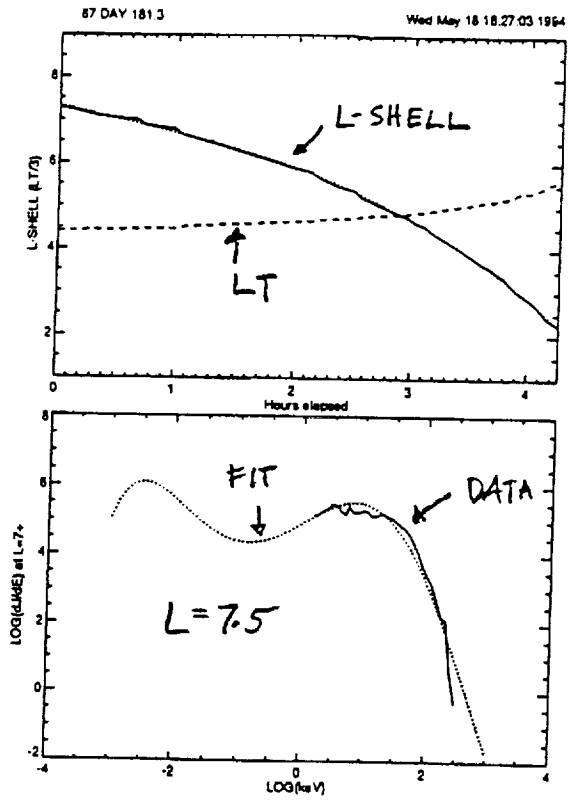
87 DAY 181.3
Wed May 18 18:27:03 1994
L-SHELL
LT
L-SHELL (LT/3)
Hours elapsed
FIT
DATA
L=7.5
LOG((dJ/dE) at L=7+
LOG(keV)

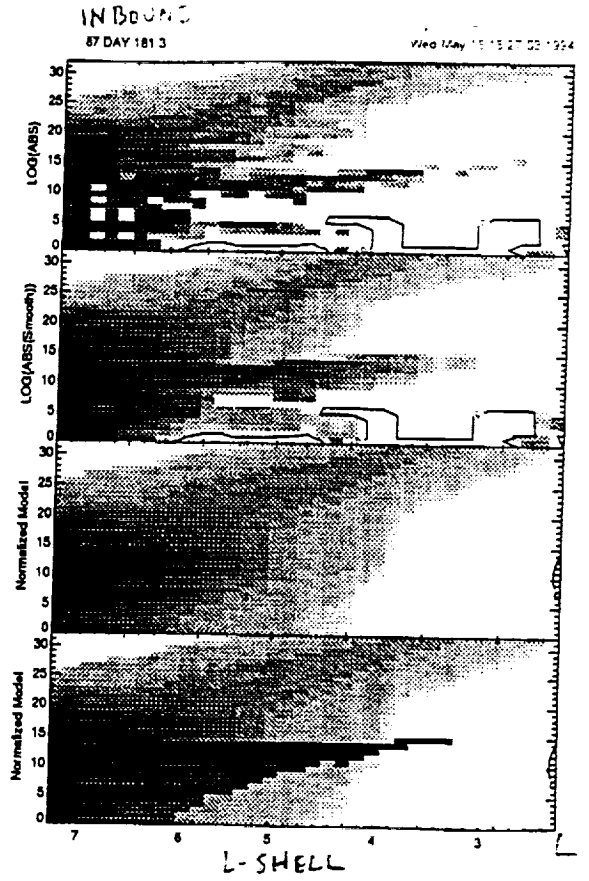
INBOUND
87 DAY 181.3
LOG(ABS)
LOG(ABS(Smooth))
Normalized Model
Normalized Model
L-SHELL

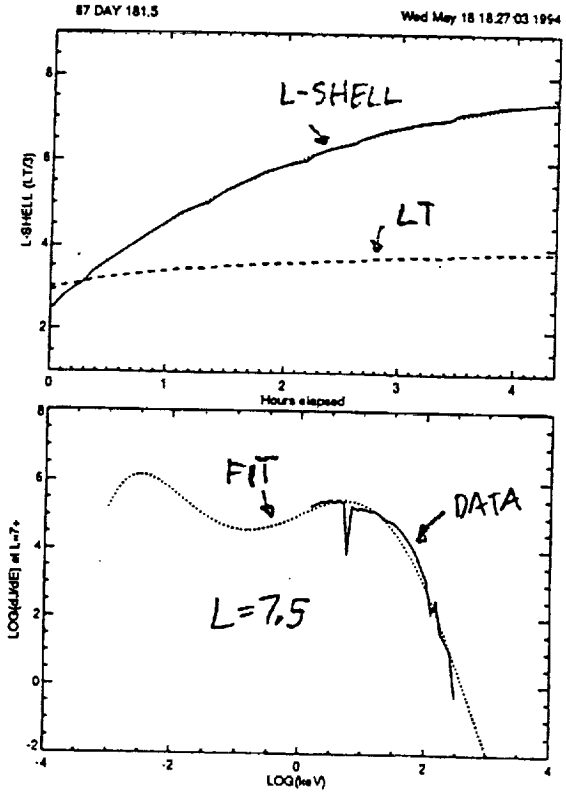
87 DAY 181.5
Wed May 18 18:27:03 1994
L-SHELL
LT
L-SHELL (LT/3)
Hours elapsed
FIT
DATA
L=7.5
LOG((dJ/dE) at L=7+
LOG(keV)

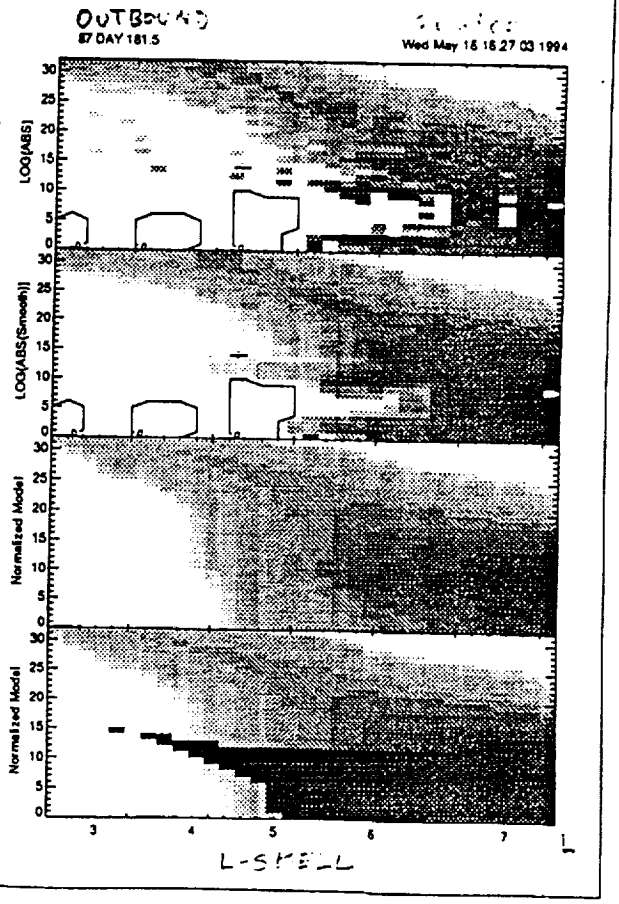
OUTBOUND
87 DAY 181.5
Wed May 18 18:27:03 1994
LOG(ABS)
LOG(ABS(Smooth))
Normalized Model
Normalized Model
L-SHELL

FIGURE 6

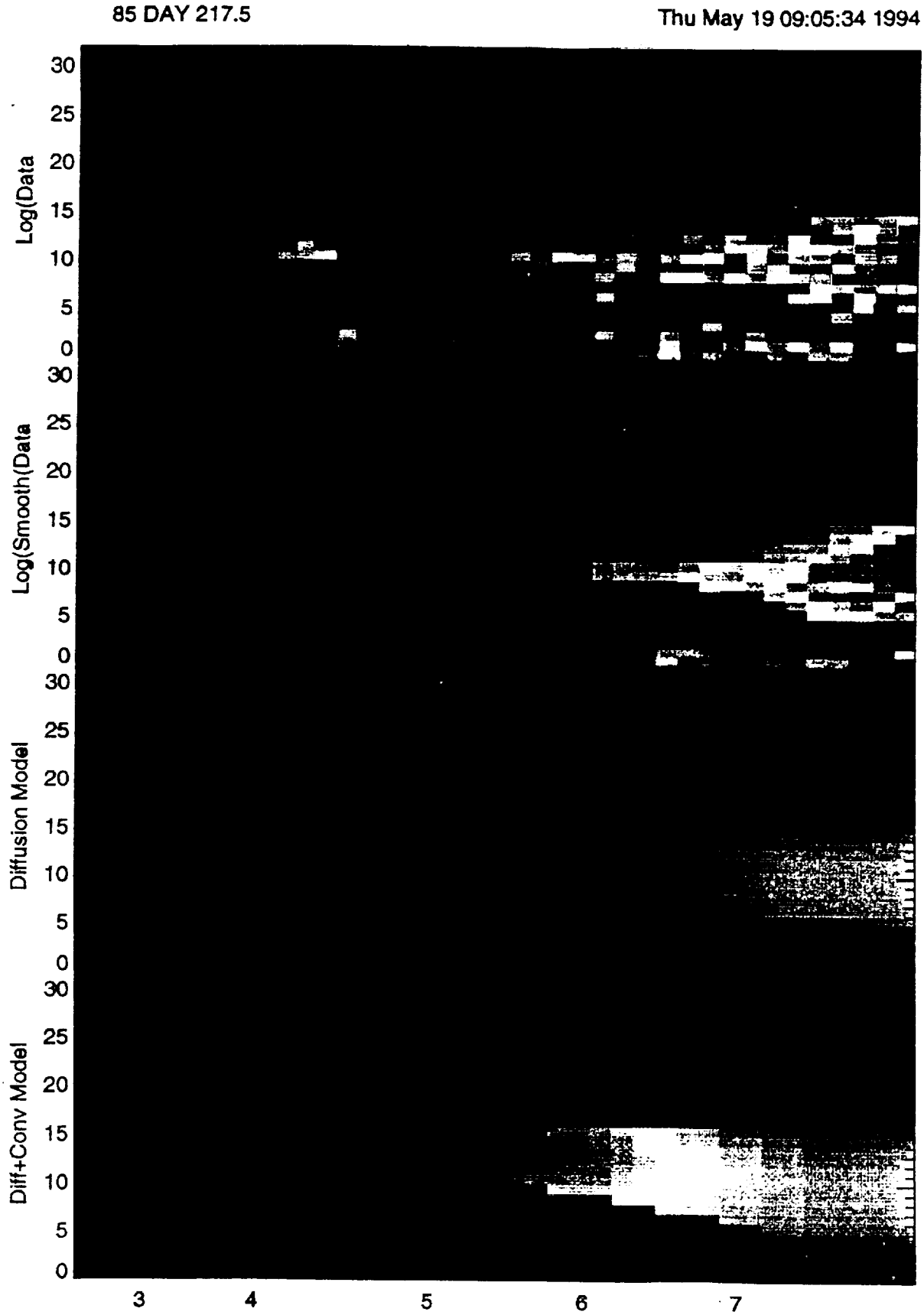

FIGURE 7 (original in color)

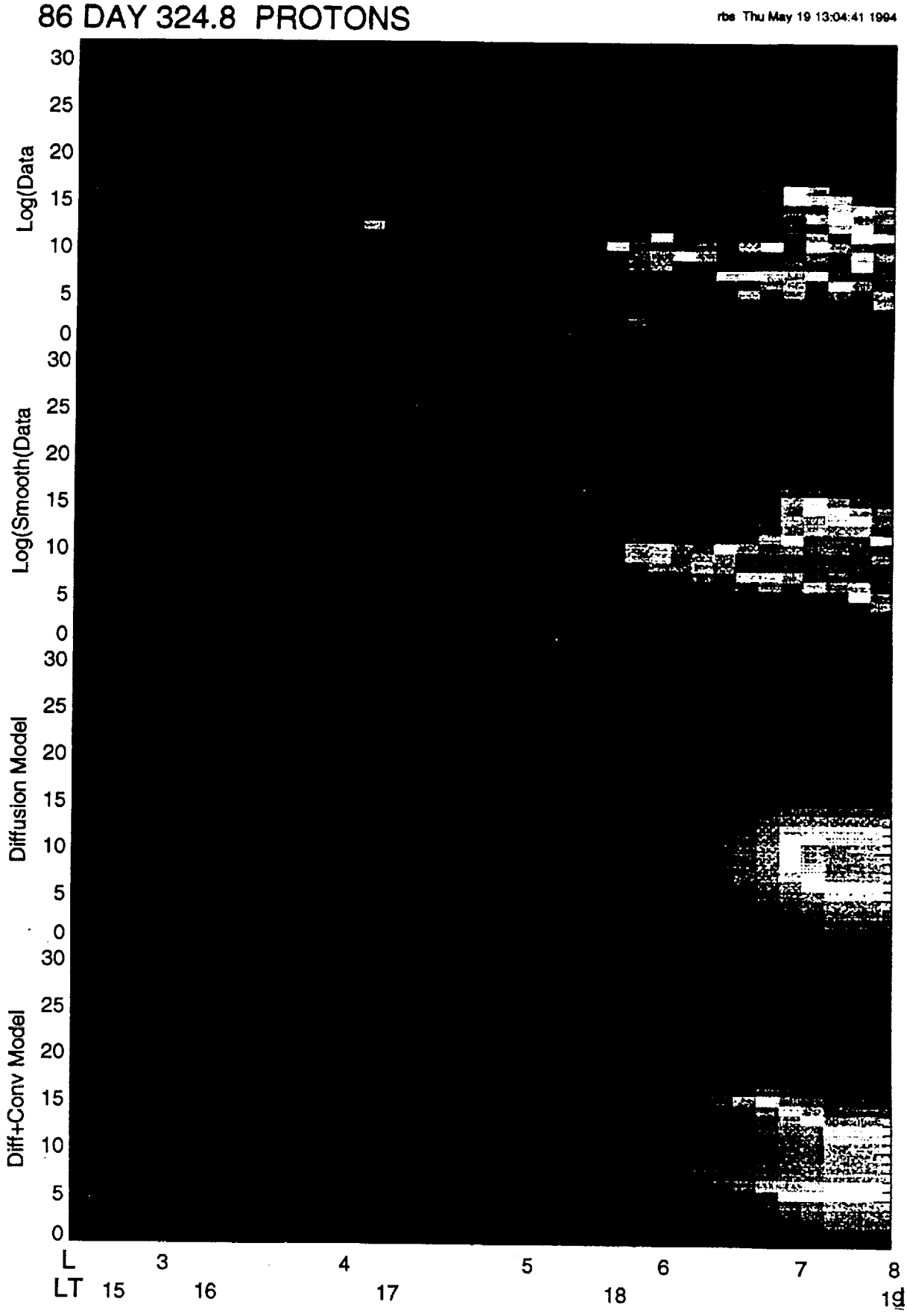

FIGURE 8 (original in color)

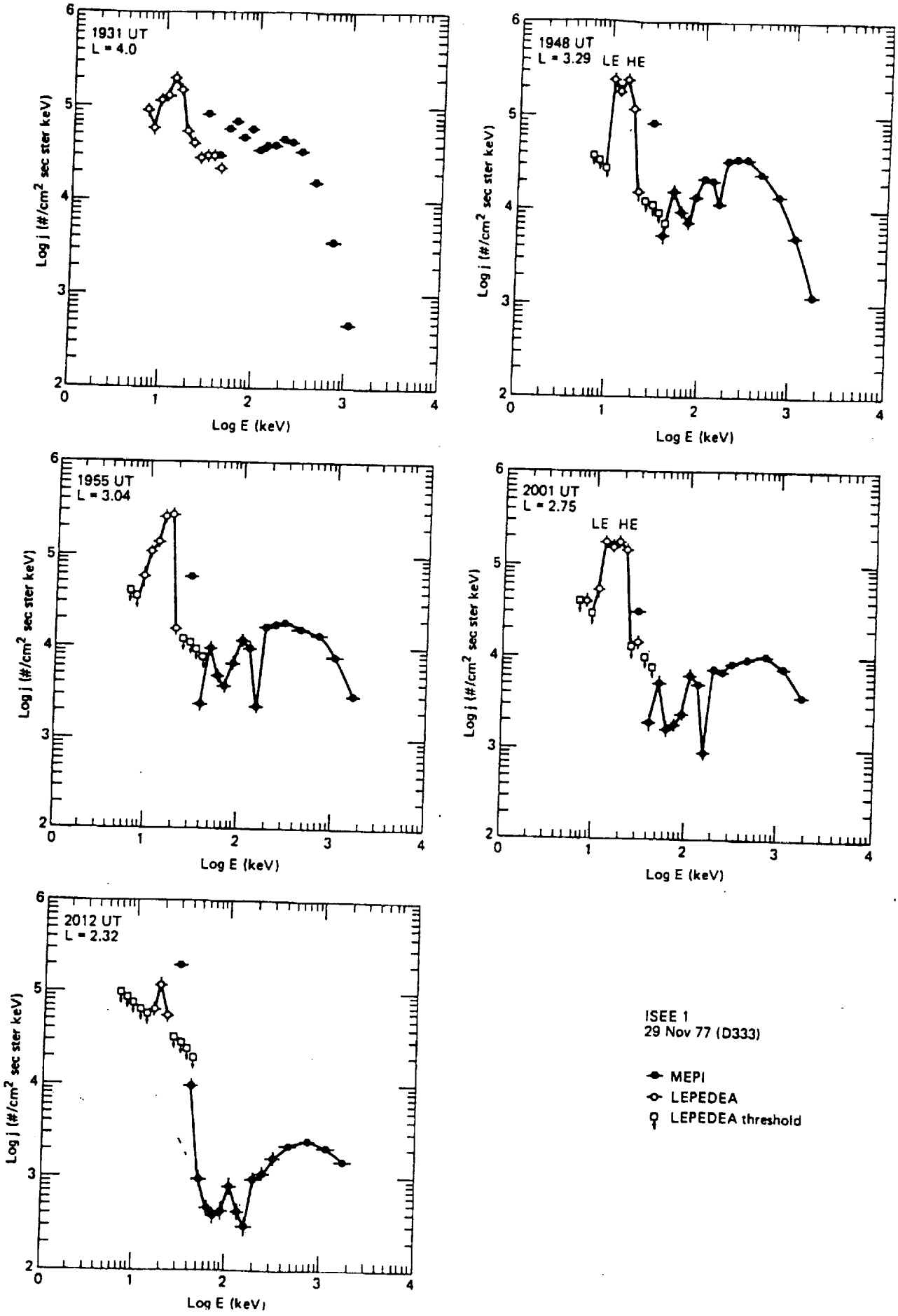
1931 UT
L = 4.0
1948 UT
L = 3.29 LE HE
1955 UT
L = 3.04
2001 UT
L = 2.75
LE HE
2012 UT
L = 2.32
Log j (#/cm² sec ster keV)
Log E (keV)
ISEE 1
29 Nov 77 (D333)
MEPI
LEPEDEA
LEPEDEA threshold

FIGURE 9

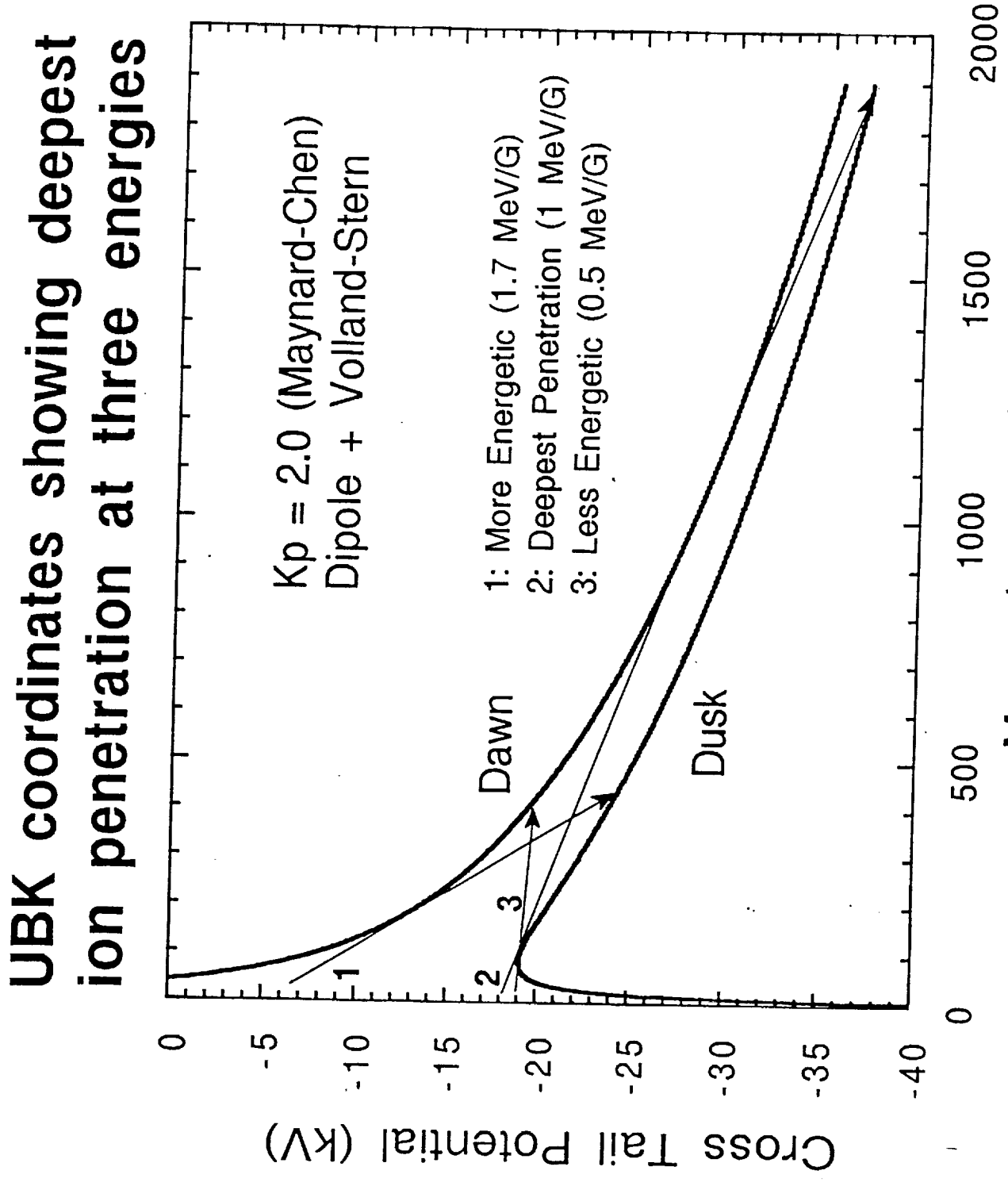
UBK coordinates showing deepest ion penetration at three energies
Kp = 2.0 (Maynard-Chen)
Dipole + Volland-Stern
1: More Energetic (1.7 MeV/G)
2: Deepest Penetration (1 MeV/G)
3: Less Energetic (0.5 MeV/G)
Dawn
Dusk
1
2
3
Cross Tail Potential (kV)
0
-5
-10
-15
-20
-25
-30
-35
-40
0
500
1000
1500
2000
Magnetic Field (nT)

FIGURE 10

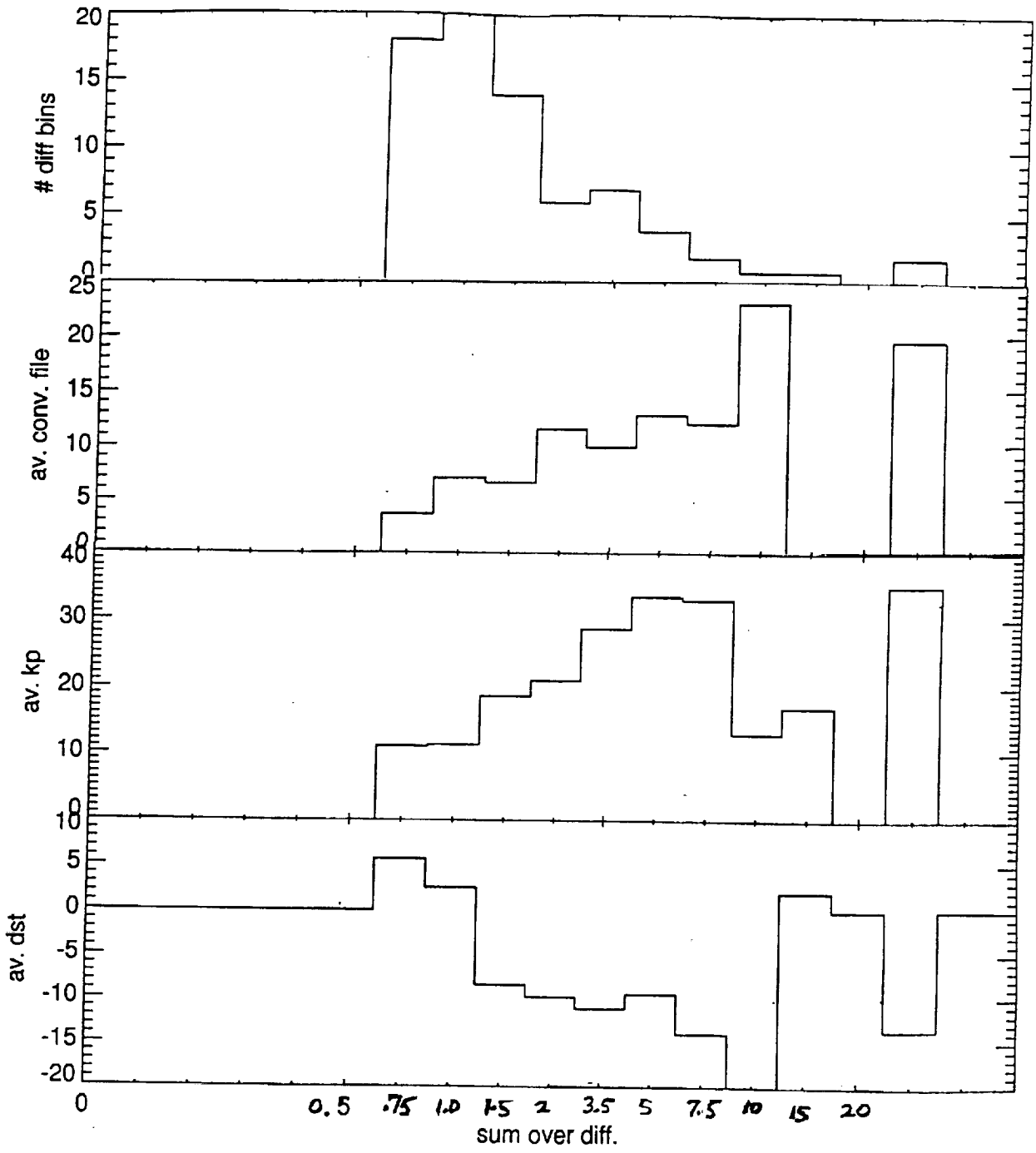

$(\times\ 3\times 10^{11}\ R_E^{2/5}\ D_{LL}^{E})$

FIGURE 11

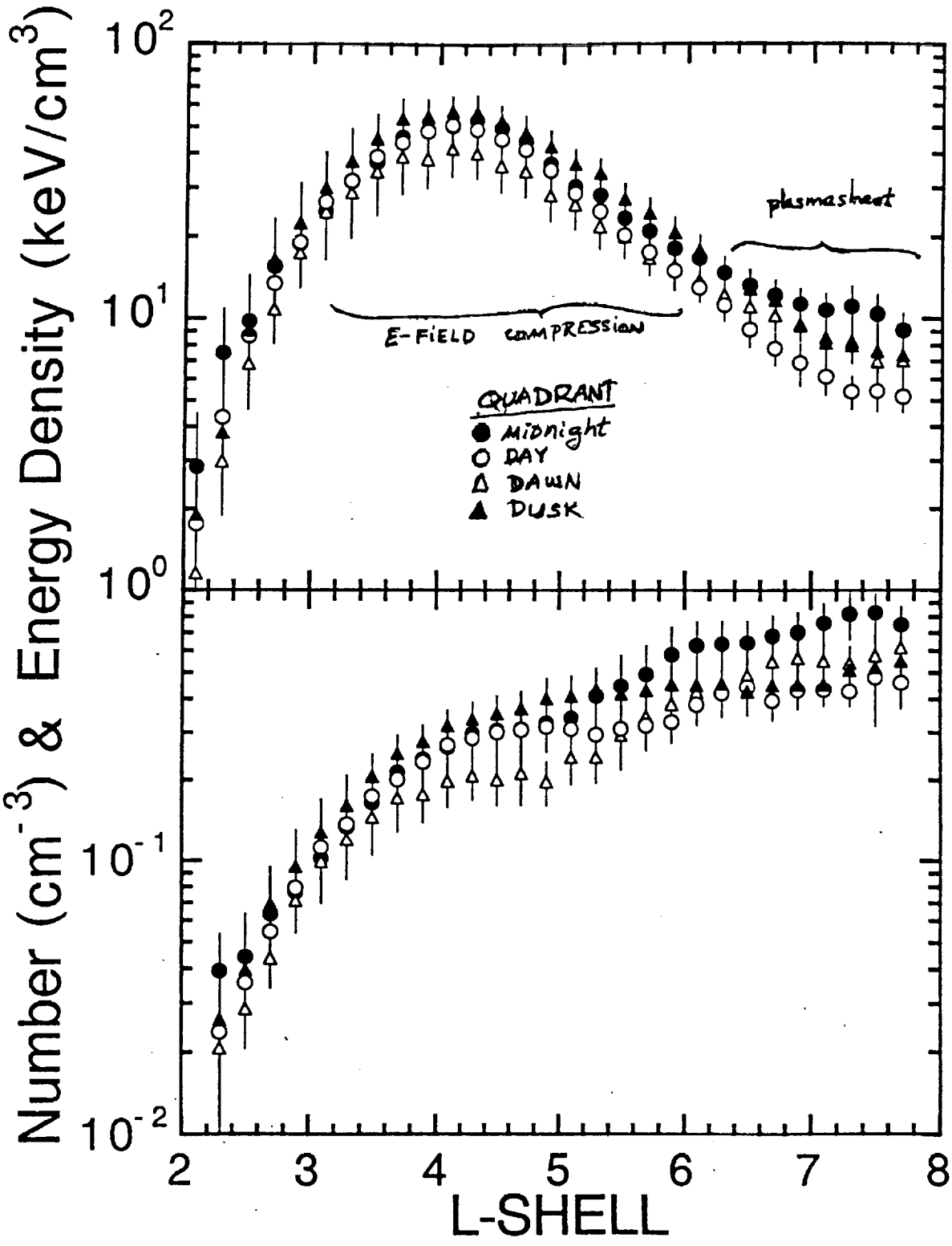
Number (cm^{-3}) & Energy Density (keV/cm^3)
10^2
10^1
10^0
10^{-1}
10^{-2}
2
3
4
5
6
7
8
L-SHELL
plasmasheet
E-FIELD COMPRESSION
QUADRANT
Midnight
DAY
DAWN
DUSK

FIGURE 12